Journal of Nuclear Materials 384 (2009) 163–174

Contents lists available at ScienceDirect

Journal of Nuclear Materials

journal homepage: www.elsevier.com/locate/jnucmat

A polycrystalline modeling of the mechanical behavior of neutron irradiated zirconium alloys

Fabien Onimus *, Jean-Luc Béchade

Service de Recherches Métallurgiques Appliquées, CEA-Saclay, 91191 Gif-sur-Yvette cedex, France

ARTICLE INFO

Article history:
Received 22 August 2008
Accepted 12 November 2008

PACS:
61.82.Bg
62.20.fq

ABSTRACT

Zirconium alloys used as fuel cladding tubes in the nuclear industry undergo important changes after neutron irradiation in the microstructure as well as in the mechanical properties. However, the effects of the specific post-irradiation deformation mechanisms on the mechanical behavior are not clearly understood and modeled. Based on experimental results it is discussed that the kinematic strain hardening is increased by the plastic strain localization inside the dislocation channels as well as the only basal slip activation observed for specific mechanical tests. From this analysis, the first polycrystalline model is developed for irradiated zirconium alloys, taking into account the irradiation induced hardening, the intra-granular softening as well as the intra-granular kinematic strain hardening due to the plastic strain localization inside the channels. This physically based model reproduces the mechanical behavior in agreement with the slip systems observed. In addition, this model reproduces the Bauschinger effect observed during low cycle fatigue as well as the cyclic strain softening.

1. Introduction

Zirconium alloys are in wide-spread use as fuel cladding tube material in light water nuclear reactors. Since the cladding is the first confinement barrier of the radioactive elements it is essential to have a good understanding and prediction of the effects of neutron radiation on the microstructure as well as on the mechanical properties.

One of the main effects of neutron radiation on metals is the creation of a high density of point defect clusters often in the form of small prismatic loops (for Zr alloys, see [1,2]). These loops are known to act as obstacles against dislocation glide leading to a strong irradiation induced hardening (for Zr alloys, see [3–5]). Nevertheless, these obstacles can be overcome by dislocations when a sufficient stress is applied, the loops being subsequently annihilated or dragged by dislocations following various possible mechanisms [6–8]. This process of removal of irradiation loops by moving dislocations produces a defect-free channel that constitutes a preferred area for further dislocation gliding. The dislocations channeling mechanism has been observed in irradiated zirconium alloys [9–16] as well as in other irradiated metals as reviewed by Wechsler [17]. However, there is yet no clear understanding of the effects of this specific deformation mechanism on the mechanical behavior of irradiated metals. In addition, very few authors [18–20] have proposed micromechanical models for the dislocation channeling phenomenon. Furthermore, to our knowledge, there is no polycrystalline model adapted to irradiated metals that takes into account the texture of the material, the intergranular stresses associated with the polycrystalline nature of the metal, as well as the specific deformation mechanisms of the irradiated metals.

In order to investigate in more detail, at the polycrystalline scale, the effects of the dislocation channeling mechanism on the mechanical behavior of irradiated zirconium alloys, various experimental data, both at the micro and at the macroscopic scale, are discussed. The origin and the detailed process of the dislocation channeling mechanism are not studied here. A polycrystalline model is then described and applied to non irradiated zirconium alloys. This polycrystalline model is adapted to irradiated zirconium alloys and adjusted on the mechanical behavior obtained on monotonic tests. The computed relative slip system activities are compared to transmission electron microscopy (TEM) observations given in the literature. Eventually, the polycrystalline model is used to compute low cycle fatigue tests that are compared to the literature data.

2. Analysis of the radiation effects on the mechanical behavior

As reviewed by Luft [21] several authors have discussed the question of the effects of channel slip on the strain and fracture behavior of neutron irradiated polycrystalline metals. It is generally assumed that the dislocation channeling is a consequence of the strain induced structural softening at the microscopic scale,

* Corresponding author. Tel.: +33 1 69 08 44 29; fax: +33 1 69 08 71 30.
E-mail address: fabien.onimus@cea.fr (F. Onimus).

0022-3115/$ - see front matter © 2008 Elsevier B.V. All rights reserved.
doi:10.1016/j.jnucmat.2008.11.006

inside the channels, due to the removal of irradiation defects. This local strain softening is usually believed to decrease the macroscopic strain hardening capacity of the material. The reduced strain hardening rate is then the cause of the small uniform elongation and the early plastic instability in the tensile deformation of neutron irradiated metals. It is also shown that the plastic instability manifests itself either in a diffuse necking or in the development of macroscopic shear bands, which cause localized shear fracture. Although the uniform elongation is dramatically reduced by irradiation, the fracture mode remains usually ductile, as pointed out by Luft [21].

Despite these general observations, the link between the occurrence of the dislocation channeling phenomenon and the appearance of shear bands at the specimen scale, associated to the macroscopic yield drop, does not seem to be clear [22]. It is indeed often ambiguously stated in the literature whether the yield drop, or the appearance of the macroscopic shear band, occurs simultaneously with the appearance of the first channels or whether channels are already present before the yield drop.

In the case of irradiated zirconium alloys dislocation channeling has been observed by various authors [9–16]. In addition another major change in the deformation mechanism has been reported. Indeed, it has been established [14–16,23] that dislocation channeling occurs only in the basal plane for internal pressure and transverse tensile tests performed at 350°C whereas mainly prism slip occurs for unirradiated zirconium alloys tested in the same conditions [14,24–27]. It is therefore believed that the large majority of the plastic strain, up to the uniform elongation, occurs by basal slip. Indeed, it has been proven by Sharp [28] that for neutron irradiated copper, the coarse slip markings that are observed at the surface of the specimen correspond to the dislocation channels demonstrating that the large majority of slip occurs inside the channels.

The reversal of the principal slip system with irradiation, in the case of zirconium alloys, is believed to be due to differences in junction reaction between irradiation induced loops and dislocations that are gliding either in the prism or in the basal slip systems [14,16,29,30]. Indeed, due to the three fold symmetry of the hexagonal closed packed (HCP) lattice, the junction created between a <*a*> loop and a <*a*> dislocation gliding in the basal plane is always glissile whereas it is sessile when the <*a*> dislocation is gliding in a prism plane. Concerning the interaction between the pyramidal <*c* + *a*> slip system and the <*a*> loops it is believed that the interaction is strong but this is still an ongoing topic of research. More generally, details of the dislocations channeling mechanism are not yet clearly understood despite recent progress in that field [31,32].

It has been shown by Fregonese et al. [14] that, for a transverse tensile test, dislocation channels in irradiated zirconium alloys are already present before the yield drop, when the plastic strain is still homogeneous at the specimen scale. This phenomenon has also been observed by Edwards et al. [22] for neutron irradiated iron. More recently accurate laser measurements (with an uncertainty lower than two micrometers) of the external diameter of the cladding have been performed after internal pressure testing [16]. It is shown that, in a part of the cladding, the deformation is homogeneous. In the homogeneously deformed zone of the cladding, thin foils have been taken and it is shown that in these thin foils dislocation channels are present. This demonstrates that the localization of the plastic strain occurs at the microscopic scale inside channels although the deformation is homogeneous at the macroscopic scale. Moreover, it has been shown in [16,23] that for a specimen deformed up to 0.2% plastic strain (referred as specimen D in [16,23]), dislocation channels are already present at this strain level and that for a specimen deformed up to 0.5% plastic strain (referred as specimen C in [16,23]), many dislocation channels are present in the material. Assuming that dislocation channels were already present in this last specimen (specimen C) at 0.2% plastic strain it can be surprising that the macroscopic flow stress increases from 0.2% plastic strain up to 0.5% plastic strain, as it is shown in [23]. Indeed, since it is commonly assumed that dislocation channeling occurs because of local strain softening, one would have expected strain softening to occur at the macroscopic scale.

In order to explain these experimental observations, it is proposed that the internal stresses, or intergranular stresses, induced by the polycrystalline nature of the material can balance, up to the uniform elongation, the local strain softening that occurs inside the channels. Furthermore, it is suggested that the plastic strain localization inside the channels and the only activation of the basal slip can induce higher internal stresses than in the non irradiated material where the slip occurs homogeneously mainly by prism glide before the activation of secondary slip systems.

Indeed, it is well known that unirradiated zirconium alloys exhibit a strong Bauschinger effect observed during tension–compression tests [33–38]. This phenomenon is attributed [33,34,37,38] to strong intergranular stresses. These strong intergranular stresses are mainly due to the strain incompatibilities between grains consequence of the plastic anisotropy of the hexagonal closed packed (HCP) crystallographic structure which presents a limited number of easy glide slip systems.

In the case of irradiated zirconium alloys, very few data concerning the Bauschinger effect are reported in the literature. Only Wisner et al. [39] have reported tension–compression curves that permit to estimate the Bauschinger effect of irradiated zirconium alloys. These authors have performed low cycle fatigue tests in the transverse direction on neutron irradiated recrystallized Zy-2 at 343 °C. It can be observed qualitatively from the stabilized hysteresis loops reported in [39] (and given in Fig. 7) that the irradiated material exhibits, in addition to the irradiation induced hardening, a stronger Bauschinger effect than the non irradiated material for a lower plastic strain level. This proves that the kinematic strain hardening is increased by irradiation. In addition, the low cycle fatigue tests performed by Wisner et al. [39] have shown that cyclic softening occurs for the irradiated material whereas a low cyclic hardening occurs for the non irradiated material. This phenomenon is attributed by the authors to the softening that occurs inside dislocation channels by analogy with channels observed in neutron irradiated copper tested in low cycle fatigue [40]. Furthermore, it has been proven [16] that during transverse tensile tests and internal pressure tests performed at 350 °C dislocation channeling occurs only in the basal plane. This shows that basal channeling probably also occurs for the low cycle fatigue tests performed in the transverse direction. Because of the limited number of slip systems (only basal slip) strong strain incompatibilities between grains are believed to occur leading therefore to high intergranular stresses that can partly explain the strong Bauschinger effect observed by Wisner et al. [39]. In addition, since the large majority of the plastic strain occurs inside the channels (of the order of 100% shear plastic strain according to Williams et al. [10]), there must also be strong strain incompatibilities between grains at the tip of the channels, at grain boundaries. This phenomenon has been underlined by Luft [21] who pointed out the presence of strong stress concentrations at grain boundaries, probably caused by the pile-up of dislocation groups. It is proposed that these strain incompatibilities between the channels and the surrounding grains induce important back stresses or microscopic internal stresses. A micromechanical model based on dislocation pile-up inside channels has been developed by Byun and Hashimoto [20]. This model highlights the importance of the long range internal stresses in irradiated metals due to the dislocation channeling process. Another approach can illustrate this phenomenon. Indeed, it has been shown by TEM observations [16] that the vol-

ume fraction of basal channels, observed for internal pressure test and transverse tensile test, increases up to 2% at 0.5% plastic strain. Since the large majority of the plastic strain occurs inside the channels, for a low amount of macroscopic plastic strain, a very large plastic strain is required inside the channels. This very high local plastic strain induces important strain incompatibilities that lead to internal stresses arising between the channels and the rest of the material that remains elastic. As a conclusion, both the only basal slip activation (for internal pressure test and transverse tensile test) and the localization of the plastic strain inside basal channels induce strong microscopic internal stresses that explain the important Bauschinger effect observed by Wisner et al. [39]. The important microscopic internal stresses are believed to balance the local strain softening that occurs inside channels, up to the uniform elongation, therefore explaining that the flow stress increases although dislocation channeling already occurs. This also explains that although dislocation channeling occurs, the plastic strain is still homogeneous at the macroscopic scale (up to the uniform elongation).

However, as the number of dislocation channels increases with plastic strain, the macroscopic strain hardening rate decreases leading to the localization of the plastic strain at the specimen scale, thus leading to the macroscopic plastic instability.

Moreover, it has been pointed out by Rosenbaum et al. [41] and Lee and Adamson [42] and reviewed by Luft [21], that shear instabilities observed for neutron irradiated metals are particularly important in the case of strongly textured material such as zirconium alloys. Indeed, in this case, coordinated propagation of the microscopically localized slip across the grain boundaries occurs as reported in [16,23]. The propagation of channels from grain to grain allows the plastic accommodation of the strong strain incompatibilities at the tip of the channels leading to a rapid decrease of the strain hardening rate as shown in [23,43]. This process eventually leads to the creation of a shear zone which penetrates the entire specimen cross section [42]. The macroscopic yield drop is believed to occur when a sufficient amount of channels are present in the material and are connected. In the shear zone it is shown by TEM observations [9,14] that the radiation damage has been fully annihilated by dislocation motion but dislocation tangles and cells are present leading eventually to a ductile failure mode [10,14].

In order to investigate in more detail, and predict, the effects of the dislocation channeling mechanism on the mechanical behavior of irradiated zirconium alloys, a polycrystalline model for the irradiated material has been developed. Firstly, the polycrystalline model used is described and applied to the unirradiated zirconium alloys. The polycrystalline model is then adapted to the irradiated zirconium alloys and adjusted on the mechanical behavior obtained on monotonic tests and then compared to TEM observations. Low cycle fatigue test results obtained by Wisner et al. [39], which are the only direct experimental evidences for the strong Bauschinger effect in neutron irradiated zirconium alloys, are then compared to computations of low cycle fatigue tests performed using the proposed polycrystalline model.

3. Polycrystalline modeling

The modeling and prediction of the mechanical behavior of polycrystals using homogenization techniques has been studied by numerous authors as reviewed by Berveiller and Zaoui [44], Kocks et al. [45], Barbe et al. [46] and Brenner et al. [47]. These polycrystalline models, based on the so-called "self-consistent scheme", are able to evaluate the effective properties of a polycrystalline aggregate from the knowledge of the behavior of its constituents. In the self-consistent framework, the geometry of the grain aggregate is not taken into account. All the grains with the same crystallographic orientation are considered as the same crystallographic phase (g) characterized by its three Euler's angles (φ_1, ϕ, φ_2) only and its volume fraction (f_g). These data are obtained experimentally by X-ray diffraction texture analysis. A list of 240 different crystallographic orientations representative of the texture of the material is chosen here (Fig. 1). In this approach, each crystallographic phase of the polycrystal can be successively regarded as an inclusion within the "matrix" made of all the crystallographic phases (homogeneous equivalent medium) submitted to homogeneous boundary conditions. The behavior of the polycrystal is then calculated by some adequate average process over all crystallographic phases. However, the self-consistent scheme leads, for anisotropic elasto-visco-plastic polycrystals, to a very complex formulation. Berveiller and Zaoui [44] have derived, from this complex formulation, a simple model, in the framework of elasto-plastic behavior, only valid in specific cases. Indeed, as described in [44,46,48], it can be shown that if homogeneous and isotropic elasticity is considered the macroscopic stress and plastic strain obey to the following equation:

$$\underline{\underline{E}}^p = \sum_{g\in G} f_g \underline{\underline{\varepsilon}}^p_g; \quad \underline{\underline{\Sigma}} = \sum_{g\in G} f_g \underline{\underline{\sigma}}_g = 2\mu\left\{\mathbf{I} + \frac{\nu}{1-2\nu}\underline{\underline{I}}\otimes\underline{\underline{I}}\right\}(\underline{\underline{E}} - \underline{\underline{E}}^p), \tag{1}$$

where μ is the shear modulus which can be computed from the Young's modulus (Y) and the Poisson's ratio (ν) as $\mu = Y/(2+2\nu)$. The macroscopic plastic strain $\underline{\underline{E}}^p$ is the average of the local plastic strain $\underline{\underline{\varepsilon}}^p_g$ over all the grains and the macroscopic stress $\underline{\underline{\Sigma}}$ can be deduced from the Hooke's law. The tensors given in the Hooke's law are defined in the Appendix. In the framework of elasto-plastic polycrystals with isotropic texture and with crystallographic phases that can be considered as spheres within the matrix, Berveiller and Zaoui [44] have developed the so-called "secant approximation" of the self-consistent scheme. These authors have shown that, in these conditions and under radial monotonic loading, the local stress and the macroscopic stress are related by a simple explicit concentration rule given by the following equation:

$$\underline{\underline{\sigma}}_g = \underline{\underline{\Sigma}} + 2\mu(1-\beta)\alpha\left(\underline{\underline{E}}^p - \underline{\underline{\varepsilon}}^p_g\right) \quad \text{with} \quad \frac{1}{\alpha} \approx 1 + \frac{3}{2}\mu\frac{\left\|\underline{\underline{E}}^p\right\|}{J_2(\underline{\underline{\Sigma}})} \quad \text{and} \quad \beta = \frac{2(4-5\nu)}{15(1-\nu)}, \tag{2}$$

The two scalar quantities $\left\|\underline{\underline{E}}^p\right\|$ and $J_2(\underline{\underline{\Sigma}})$ are defined in Appendix.

It can be seen that at the beginning of the deformation, the α factor is close to 1 and decreases as the plastic deformation proceeds, accounting for the plastic accommodation between grains. As pointed out by Hoc and Forest [48] the concentration rule proposed by Berveiller and Zaoui [44] is suitable for monotonic load-

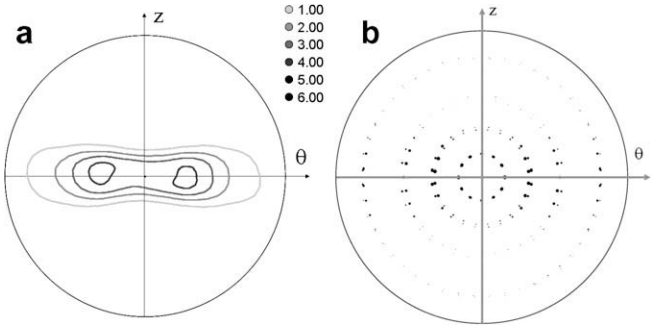

Fig. 1. (a) {0002} experimental pole figure of a recrystallized zirconium alloy cladding tube, (b) {0002} pole figure of the 240 orientations used to describe the texture of the recrystallized zirconium alloy cladding tube. The surface of the spot is proportional to the volume fraction of each crystallographic orientation.

ing applied to isotropic polycrystals but does not allow the simulation of changes of loading path in textured polycrystals. In order to keep the advantage of a concentration rule that can be expressed explicitly and in order to extend the field of applications of this type of model, Cailletaud [49] and Pilvin [50] have postulated, an explicit concentration rule given in the following equations:

$$\underline{\underline{\sigma}}_g = \underline{\underline{\Sigma}} + 2\mu(1-\beta)\left(\underline{\underline{B}} - \underline{\underline{\beta}}_g\right) \quad \text{with} \quad \underline{\underline{B}} = \sum_{g\in G} f_g \underline{\underline{\beta}}_g, \tag{3}$$

$$\dot{\underline{\underline{\beta}}}_g = \dot{\underline{\underline{\varepsilon}}}^p_g - D\left(\underline{\underline{\beta}}_g - \delta\underline{\underline{\varepsilon}}^p_g\right)\left\|\dot{\underline{\underline{\varepsilon}}}^p_g\right\|. \tag{4}$$

The new second rank tensor internal variable β_g is a local internal variable that evolves non-linearly with the local plastic strain of the crystallographic phase, according to Eq. (4). The evolution law of this internal variable is inspired by the non linear evolution of the kinematic strain hardening used in macroscopic models [51]. The effect of this non linear evolution of this internal variable is to account for the plastic accommodation between grains, like the α factor in the Berveiller–Zaoui (B–Z) model. The tensor formulation is able to give a suitable description of cyclic tests. This model, referred here as the Cailletaud–Pilvin (C–P) model, has no justification from the homogenization theory point of view but corresponds to an empirical approximation of the self-consistent scheme. Indeed, the authors [50] have proposed to adjust both parameters D and δ of the evolution law of the internal variable $\underline{\underline{\beta}}_g$ on the local mechanical response of the self-consistent B–Z model. More precisely, ten different crystallographic orientations (Fig. 2(b)) are chosen within the list of 240 orientations used for the simulation of the behavior of the material. For these ten different orientations, the stress and strain are computed during the simulation for both the B–Z and the C–P model. Using a mean square minimization procedure, the two parameters, D and δ, are adjusted and the difference between the stress and strain computed by the B–Z and the C–P model for the ten orientations is minimized. Since the B–Z model is a self-consistent model based on the "secant approximation", the Cailletaud–Pilvin (C–P) model is therefore very close, both at the micro and at the macroscopic scale, to the self-consistent "secant" response. Nevertheless, the two parameters, D and δ, have to be adjusted on the B–Z model in the appropriate conditions. Indeed, the B–Z model is restricted to the elasto-plastic behavior, thus only the elasto-plastic behavior can be simulated using this approach. The B–Z model is also limited to monotonic proportional loading paths and isotropic textures, therefore the adjustment of the two parameters, D and δ, of the C–P model on the local response of the B–Z model have to be performed during a monotonic proportional loading with an isotropic texture (Fig. 2(a)). But since the C–P model is suitable to simulate non-monotonic loading, the authors [50] have proposed to use the C–P model to compute cyclic tests, with the D and δ parameters adjusted on the B–Z model during a monotonic test. The authors have also proposed to go further by extrapolating the C–P model to non-isotropic textures. The two parameters D and δ are adjusted on the B–Z model during a monotonic loading with an isotropic texture, but once these two parameters are obtained, non-monotonic tests on a non-isotropic texture can be computed. Indeed, the D and δ parameters are characteristic of the plastic accommodation rate of the intergranular stresses for each phase, as for the α factor in the B–Z model, regardless of its orientation. Changing the texture of the material does not change the plastic accommodation rate of each phase.

This extrapolation considerably extends the field of applications of this simple polycrystalline model and allows simulating the mechanical behavior of textured zirconium alloys during cyclic tests.

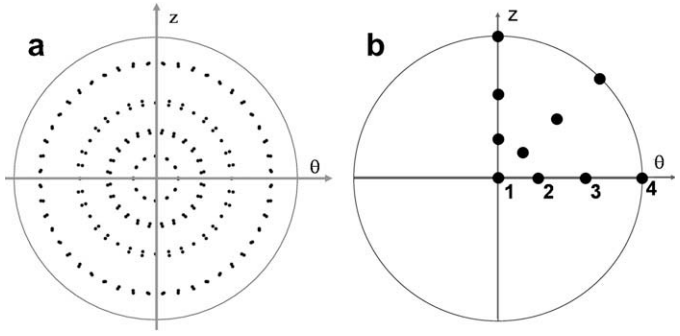

Fig. 2. (a) {0002} pole figure of the 240 orientations describing the isotropic texture used for the adjustment of the C–P model on the self-consistent B–Z model. The surface of the spot is proportional to the volume fraction of each crystallographic orientation. (b) {0002} pole figure of the 10 crystallographic orientations used for the adjustment of the C–P model on the self-consistent B–Z model.

4. Polycrystalline modeling of the mechanical behavior of unirradiated recrystallized Zr alloys

4.1. Polycrystalline modeling applied to Zr alloys

Various polycrystalline models have been applied to α-zirconium which is often considered as a textbook case for self-consistent approaches due to its strong plastic anisotropy. From the early work of Hutchinson [52] followed by a large body of work from Lebensohn and Tomé [53] and Turner et al. [54,55] up to recent developments [47], important efforts have been made to improve the prediction of the mechanical response of zirconium alloys both at the macroscopic and at the microscopic scale [56] using the most accurate, but complex, models. These approaches have proven to be very valuable especially in the case of thermal creep [27,56] of recrystallized zirconium alloys tested at 400 °C. At the same time, the simple Cailletaud–Pilvin (C–P) model has been applied by Geyer [57,58] to model the behavior of the unirradiated recrystallized Zy-4 at room temperature. Fandeur et al. [59] have also applied the same type of modeling to the unirradiated as well as the irradiated cold-work stress relieved Zy-4 tested at 350 °C. More recently, developments [23] have been proposed in order to take into account the dislocation channeling mechanism, for the irradiated material, into the polycrystalline modeling. However, the explicit introduction of the geometry of channels turned out to be very complex. For the present purpose, a novel approach is proposed for the modeling of the mechanical behavior of the irradiated recrystallized zirconium alloys tested at 350 °C. This approach is based on well established homogenization procedure and well known intra-granular behavior.

4.2. Plastic deformation modes of zirconium alloys

As reviewed by Douglass [24] and Tenckhoff [25], in the α structure of zirconium two major deformation modes can be activated: slip and twinning. According to various authors [14,26,28] for recrystallized Zy-4 or M5® deformed up to 4% plastic strain at 350 °C twinning is rarely observed. At this temperature the deformation is known to occur mainly by slip on the $\{10\bar{1}0\}$ first order prism slip planes along the $\langle 11\bar{2}0\rangle$ direction of the HCP lattice, corresponding to dislocations with <a> type Burgers vector. The basal {0001} and the first order pyramidal $\{10\bar{1}1\}$ slip systems with <a> Burgers vectors are also known [25] to operate in zirconium alloys. As reviewed by Tenckhoff [25], numerous evidences for <c + a> glide are reported in the literature. Indeed, this slip system is very important since it allows the accommodation of the plastic strain in the <c> direction as opposed to the other slip systems. According

to Akhtar [60], Merle [61] and Numakura et al. [62], <c + a> glide occurs on first order pyramidal slip systems. In the case of rolled sheet or cladding tubes made of industrial recrystallized zirconium alloys, it has been shown by various authors [58,14,26,27] that prism slip is mainly activated, the first order pyramidal <a> glide being the cross-slip system. According to these authors basal <a> slip and first order pyramidal <c + a> slip are observed sporadically at low plastic strain, but become important as plastic strain increases.

Four types of slip systems are therefore taken into account in the model: the three prism slip systems, the three basal slip systems, the six first order pyramidal slip systems with <a> Burgers vector and the twelve first order pyramidal slip systems with <c + a> Burgers vector.

The geometry of the slip systems of the HCP lattice is taken into account explicitly in the modeling by defining the orientation of the normal of the slip planes ($\underline{n}_s$) and the slip directions ($\underline{m}_s$) into the crystal frame. The orientation of the crystal frame with respect to the specimen frame is given by the three Euler's angles (φ_1, ϕ, φ_2) for each crystallographic phase (g). A set of 240 orientations (φ_1, ϕ, φ_2, f_g) describing the texture of the material is used. It can be seen on Fig. 1 that the orientation set is representative of the texture of the recrystallized zirconium alloys cladding, either Recrystallization Annealed (RXA) Zy-4 or M5®. Indeed the textures measured for these two materials are very similar. For the adjustment of the C–P model on the B–Z model, an isotropic texture is used (Fig. 2(a)).

4.3. Crystal plasticity constitutive laws

The condition of activation of a slip system (s) of phase (g) is such that when $|\tau_s| < \tau_s^c$ no slip occurs but when $|\tau_s| \geqslant \tau_s^c$ slip occurs on the slip system (s). The coefficient τ_s^c is the Critical Resolved Shear Stress (CRSS) of the slip system (s).

The resolved shear stress τ_s on the slip system (s) of phase (g) can be computed as Eq. (5) from the local stress given by the concentration rule (Eqs. (2)–(4))

$$\tau_s = \frac{1}{2}\underline{\underline{\sigma}}_g : (\underline{n}_s \otimes \underline{m}_s + \underline{m}_s \otimes \underline{n}_s), \tag{5}$$

where the normal direction of the slip plane ($\underline{n}_s$) and the slip direction ($\underline{m}_s$) are expressed in the specimen frame. Details of the notation are given in the Appendix.

It has been assessed experimentally [38,63,43] that unirradiated recrystallized zirconium alloys undergo very low isotropic strain hardening. The CRSS (τ_s^c) are therefore believed to increase very slowly with plastic strain. For the sake of simplicity, it is chosen that the CRSS are constant with plastic strain. Additionally, it has been shown that the deformation occurs homogeneously at the grain scale for low plastic strain level [27,58,26], as seen by the homogeneous dislocation microstructure and the homogeneous distribution of slip lines observed on the surface. Thus, intra-granular kinematic strain hardening is not believed to occur for non irradiated recrystallized zirconium alloys tested up to low plastic strain levels (<5%). The strong kinematic strain hardening observed experimentally is thus only due to strain incompatibilities between grains. These strain incompatibilities between grains are computed thanks to the polycrystalline model.

As pointed out, the approach proposed here is restricted to elasto-plastic behavior. However, a visco-plastic framework is chosen for the expression of the local constitutive behavior, in order to avoid problems related with the determination of the active slip systems in plastic models [49]. A low strain rate sensitivity is therefore adopted for the constitutive flow law, in order to benefit from the numerical advantage of the visco-plastic formulation while remaining in the case of a quasi elasto-plastic behavior. Besides, it is known that recrystallized zirconium alloys exhibit a low strain rate sensitivity around 350 °C [23] during strain hardening tests.

The flow law expressed at the slip system scale is chosen as a power law given in Eq. (6) and the critical resolved shear stresses are chosen as constant with plastic strain

$$\dot{\gamma}_s = \left\langle \frac{|\tau_s| - \tau_s^c}{K} \right\rangle^n \operatorname{sign}(\tau_s). \tag{6}$$

The notations are defined in the Appendix. Both coefficients, K and n, of the flow law (Eq. (6)) are chosen respectively equal to $K = 5$ MPa $s^{1/n}$ and $n = 10$. These two coefficients are kept fixed in the following. With these coefficients, an increase of the applied strain rate from $10^{-6}\,s^{-1}$ up to $10^{-4}\,s^{-1}$ induces an increase of the flow stress at 0.2% plastic strain lower than 1 MPa, confirming that the chosen model is quasi elasto-plastic. This therefore allows the adjustment of the C–P model on the self-consistent B–Z model which is restricted to elasto-plastic behavior.

From the computation of the slip rate on each slip system, the plastic strain rate second rank tensor of each crystallographic phase can eventually be deduced according to the following equation:

$$\underline{\underline{\dot{\varepsilon}}}_g^p = \frac{1}{2}\sum_{s\in S} \dot{\gamma}_s(\underline{n}_s \otimes \underline{m}_s + \underline{m}_s \otimes \underline{n}_s). \tag{7}$$

4.4. Refinement procedure

The model has eight fitting coefficients:

- the Young's modulus (Y) and the Poisson's ratio (ν),
- the four CRSS ($\tau_P^c, \tau_{\pi<a>}^c, \tau_B^c, \tau_{\pi<c+a>}^c$) of the four families of slip systems (prism, first order pyramidal <a>, basal and first order pyramidal <c + a>),
- the two tuning parameters, D and δ, for the empirical concentration rule.

The coefficients are fitted on the mechanical behavior of the unirradiated recrystallized zirconium alloys, RXA Zy-4 and M5® cladding tube obtained at 350 °C. Indeed the tensile behaviors of these two materials are very similar despite the difference in the alloying elements content. This is due to the fact that the grain microstructure, the dislocation microstructure as well as the texture are very similar for these two materials. The cladding tubes are approximately 0.6 mm thick with an external diameter close to 9.5 mm. The tests are performed on various recrystallized Zr alloys up to 1.5% total strain at a strain rate of $2 \times 10^{-4}\,s^{-1}$, in transverse tensile (or pure hoop direction, with $\Sigma_{rr} \approx 0$, $\Sigma_{\theta\theta}$, $\Sigma_{zz} = 0$), internal pressure ($\Sigma_{rr} \approx 0, \Sigma_{\theta\theta}, \Sigma_{zz} = \Sigma_{\theta\theta}/2$) and axial tensile ($\Sigma_{rr} = 0, \Sigma_{\theta\theta} = 0, \Sigma_{zz}$) loading conditions. Tests conditions are given in Table 1. The hoop stress is computed by using the usual thin wall formula. The transverse tensile test is performed on a cladding in the hoop direction only by using a biaxial mechanical test device allowing the application of both an axial compression loading and an internal pressure loading at the same time. A pure hoop tensile test can therefore be performed with this device.

The tests are simulated using the texture characteristic of a recrystallized zirconium alloy cladding (Fig. 1) and the adjustment of the six material coefficients are performed on the macroscopic mechanical behavior. Simultaneously, a transverse tensile test ($\Sigma_{rr} = 0, \Sigma_{\theta\theta}, \Sigma_{zz} = 0$) is simulated, using an isotropic texture (Fig. 2(a)), with both the B–Z and the C–P models. This allows the fitting of both parameters D and δ on the local stress and strain obtained by the B–Z model for ten different crystallographic orientations. The {0002} pole figure for the ten crystallographic orien-

Table 1
Irradiation and test conditions of the specimens used for the modeling.

Test	Material	Fluence (nm^{-2})	Irradiation temperature	Strain rate (s^{-1})	Test temperature
Transverse [57]	RXA Zy-4	–	–	2.0×10^{-4}	350 °C
Internal pressure [43]	M5®	–	–	2.0×10^{-4}	350 °C
Axial [57]	RXA Zy-4	–	–	2.0×10^{-4}	350 °C
Transverse (ring) [23]	RXA Zy-4	3.1×10^{25}	350 °C	1.6×10^{-4}	350 °C
Internal pressure [43]	M5®	3.5×10^{25}	350 °C	3.0×10^{-4}	350 °C

tations chosen is given on Fig. 2(b). The tests simulation and the refinement procedure are performed using the SIDOLO program described in [64]. The slip systems activities (A_s) are also computed during the simulation and compared to TEM observations. The relative slip system activities (e.g. for prism slip) are defined as the sum of the modulus of the slip rate of all three prism slip systems for each crystallographic phase, then averaged over the whole polycrystal and eventually normalized

$$A_P = \frac{1}{\sum_{i \in S} A_i} \sum_{g \in G} f_g \sum_{s \in P} |\dot{\gamma}_s|. \quad (8)$$

When refining the four CRSS, a special attention is paid to the fact that the majority of slip occurs by prism glide, the other slip systems being less activated, thus imposing that the prism CRSS is lower than the other CRSS. For the computation of the internal pressure tests, an iterative procedure is used in order to ensure that the applied axial stress (Σ_{zz}) is equal to half of the computed hoop stress ($\Sigma_{zz} = \Sigma_{\theta\theta}/2$), the hoop strain rate ($\dot{E}_{\theta\theta}$) remaining constant during the simulation.

4.5. Results of the refinement

The coefficients obtained after the refinement are given in Table 2. It can be first noticed on Fig. 3 that thanks to the two tunable parameters D and δ, the local stress and plastic strain for four out of the ten different crystallographic orientations obtained by the C–P model with an isotropic texture are in relatively good agreement with the local response computed with the B–Z model. This ensures that the C–P model is close to a secant self-consistent model. Simulated and experimental stress–strain curves are compared on Fig. 4. In the case of the internal pressure test, the hoop stress and hoop strain are plotted. It can be seen that the tests performed in the transverse tensile and internal pressure loading conditions are correctly reproduced by the model. However the computed flow stress during the axial tensile test is slightly lower than the experimental flow stress. The refined CRSS are in good agreement with the values obtained by Brenner et al. [27] in the case of thermal creep performed at 400°C on recrystallized Zr–Nb1%–O alloys.

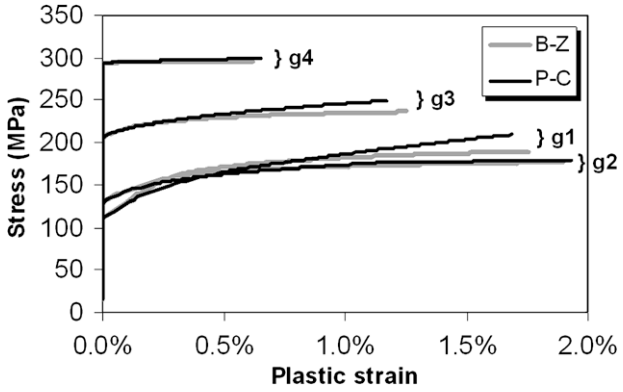

Fig. 3. Stress–plastic strain curves of four grains used for the adjustment of the C–P model on the self-consistent B–Z model. In gray lines is shown the B–Z model local response and in black lines the C–P model local response. The computed stress is a transverse tensile test.

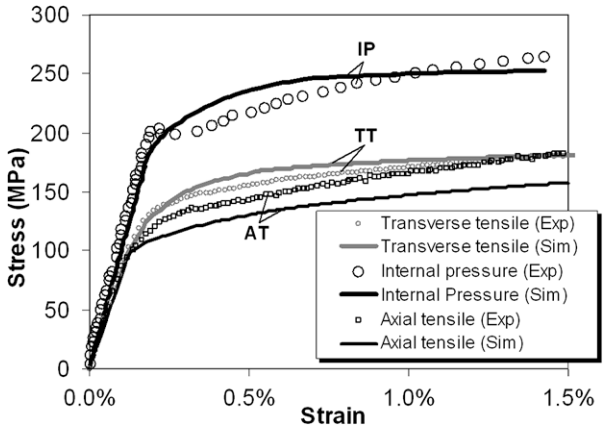

Fig. 4. Experimental (Exp) and Simulated (Sim) stress–strain curves of the Transverse Tensile test (TT), the Internal Pressure test (IP) and the Axial Tensile test (AT) for the non irradiated material.

Table 2
Coefficients obtained after the refinement for the unirradiated material.

Parameter	Value
Y (MPa)	80 000
ν	0.4
n^*	10
K^* (MPa $s^{1/n}$)	5
τ_P^c (MPa)	45
$\tau_{\pi<a>}^c$ (MPa)	60
τ_B^c (MPa)	85
$\tau_{\pi<c+a>}^c$ (MPa)	140
D	260
δ	0.26

* Fixed coefficients.

Table 3
Slip systems activities obtained at E^p = 1% for the unirradiated material. In bold letters are indicated the principal slip systems.

Activity	Transverse tensile	Internal pressure	Axial tensile
A_P	**46%**	8%	**77%**
$A_{\pi<a>}$	32%	25%	20%
A_B	16%	**44%**	3%
$A_{\pi<c+a>}$	6%	23%	0%

The relative slip system activities computed for the tests at 1% macroscopic plastic strain are given in Table 3 (hoop plastic strain

is considered for the internal pressure test). Relative activities computed for axial tensile test and transverse tensile test show that mainly prism slip is activated (respectively 77% and 46%), in good agreement with TEM results. However, it is shown that for internal pressure test prism slip activity, due to the orientation of the slip systems, is very low (8%) and activities of secondary slip systems are high, especially the basal slip (44%). This shows that the model leads to an over-estimation of the secondary slip systems activation, especially in the case of internal pressure test, whereas the prism slip system is not sufficiently activated. This phenomenon can be mainly due to the homogenization procedure, based on the secant formulation of the self-consistent problem, that can be too "stiff" according to various authors [65,66,27], leading to an over-estimation of the secondary slip systems activation. More recently, advanced polycrystalline models, such as affine, or second order self-consistent estimates, have been proposed [47,67–69]. These models give a better description of the interactions between the grains and therefore a better estimation of the activation of the secondary slip systems.

5. Polycrystalline modeling of the mechanical behavior of irradiated recrystallized Zr alloys

The polycrystalline model developed for the unirradiated recrystallized zirconium alloys can be adapted to the irradiated zirconium alloys by taking into account the mechanisms described in the first part of the paper. The homogenization procedure used to compute the mechanical response of the polycrystal from the knowledge of the intra-granular behavior is not modified. Only the intra-granular constitutive laws are adapted in order to take into account the radiation effects.

5.1. Intra-granular constitutive behavior

5.1.1. Irradiation induced hardening

It is known that the radiation induced loops act as obstacles against dislocation glide in the same way as forest dislocations. This therefore leads to an increase of the critical resolved shear stresses for all slip systems. According to the classical dispersed barrier hardening model [70,8,71] the increase of the critical resolved shear stress can be expressed as

$$\Delta\tau = \alpha\mu b\sqrt{Nd}, \tag{9}$$

where μ is the shear modulus (in MPa), N is the loop density (in m^{-3}), d is the loop diameter (in m), b is the Burgers vector (in m) and α is a proportionality factor characteristic of the strength of the obstacle.

In the case of recrystallized zirconium alloys irradiated in PWR conditions, it is shown that the loop density increases up to $N_0 = 5 \times 10^{22}\ m^{-3}$ with a mean loop diameter of $d = 10$ nm according to Régnard et al. [15] and seems to saturate for fluences above $5 \times 10^{25}\ nm^{-2}$. In the model, the values for N_0 and d are kept fixed in the following and are chosen as $N_0 = 5 \times 10^{22}\ m^{-3}$ and $d = 10$ nm.

Due to the differences in the interaction between loops and dislocations gliding either in the basal plane or in other planes, the increase in the critical resolved shear stresses (CRSS) is believed to be different for each slip system. This can be taken into account by introducing different obstacle strength for each slip system. The irradiation induced hardening is therefore modeled according to the following equation:

$$\tau_s^c = \tau_s^{c0} + \Delta\tau_s^c = \tau_s^{c0} + \alpha_s\mu b\sqrt{\rho_l} \quad \text{with} \quad \rho_l = Nd. \tag{10}$$

5.1.2. Softening behavior at the grain scale

Due to the progressive cleaning of irradiation defects by basal channeling, softening occurs inside the channels. An intra-granular softening behavior is therefore introduced at the grain scale. Since full clearing of loops only occurs inside basal channels, only the basal CRSS is assumed to be affected by the strain softening, the other CRSS remaining constant with plastic strain (Eqs. (11) and (12)) in a first approximation

$$\tau_B^c = \tau_B^{c0} + \alpha_B\mu b\sqrt{\rho_l} \quad \text{with} \quad \rho_l = Nd. \tag{11}$$

$$\tau_s^c = \tau_s^{c0} + \Delta\tau_s^c \quad \text{with} \quad \Delta\tau_s^c \quad \text{being constant for } s \neq B. \tag{12}$$

The clearing up process can be modelled, as proposed by Rodney et al. [18] and Pokor et al. [72], by considering that all the loops lying within a given distance ($H/2$) to the dislocation plane (basal plane in this case) are captured and cleared up by the dislocation. Taking into account the dislocation density ρ inside the channel gliding at the velocity $\overline{v}$, it is shown that during a time dt, the number of cleared loops inside the channel is $NH\rho\overline{v}dt$. From the Orowan equation ($\dot{\gamma} = \rho b\overline{v}$), the number of loops cleared up inside the channel during the time dt can be expressed as $\frac{H}{b}N\dot{\gamma}dt$. Therefore, the equation governing the evolution of the loop linear density (or $\rho_l = Nd$) can be deduced, written here (Eq. (13)) in a more general way by adding the contribution of all the dislocations gliding on the three basal slip systems ($s \in B$)

$$\frac{d\rho_l}{dt} = -k_B\rho_l\left[\sum_{s\in B}|\dot{\gamma}_s|\right] \tag{13}$$

with $\rho_l = Nd$, $\rho_l(0) = N_0 d$, $k_B = H/b$, $N_0 = 5\times10^{22}\ m^{-3}$ and $d = 10$ nm.

5.1.3. Intra-granular kinematic strain hardening and flow law

The analysis of various experimental data described in the first part of the paper has pointed out the importance of the kinematic strain hardening induced by the localization of the plastic strain inside the channels. This additional kinematic strain hardening can be simply taken into account at the intra-granular scale by introducing, as proposed in [73,46], a non linear kinematic strain hardening term into the flow law, similar to the Armstrong–Frederick law [74], as shown in Eqs. (14) and (15). Since only fully cleared basal channels are observed the intra-granular kinematic hardening is believed to affect only the basal slip system, in a first approximation

$$\dot{\gamma}_s = \left\langle \frac{|\tau_s - x_s| - \tau_s^c}{K} \right\rangle^n \mathrm{sign}(\tau_s - x_s) \tag{14}$$

with $x_s = 0$ for non basal slip systems ($s \neq B$) and $\dot{x}_s = C_B\dot{\gamma}_s - D_B x_s|\dot{\gamma}_s|$ for the basal slip systems ($s \in B$), with

$$x_s(t=0) = 0. \tag{15}$$

The equations of the model are recalled in the Appendix as well as the variables and the coefficients. It can be noticed that in this first approach, the dislocation channeling occurring in the prismatic and in the pyramidal planes, only observed for axial tensile test [16], have not been taken into account. Indeed, in this first approach only internal pressure tests and transverse tensile tests are simulated and for these two tests, only basal channels have been observed. Moreover, as pointed in [16], inside prismatic and pyramidal channels the defects did not seem to be fully cleared. Therefore, the softening as well as the intra-granular kinematic hardening is assumed to be lower in that case. An improvement of the modeling could probably be obtained by introducing a low softening as well as a low intra-granular kinematic hardening for prismatic and pyramidal slip.

5.2. Refinement procedure

The model has now nine fitting coefficients:

- three coefficients for the constant increment in the CRSS (for the prism ($\Delta\tau^c_P$), the pyramidal <a> ($\Delta\tau^c_{\pi<a>}$) and the pyramidal <c + a> slip systems ($\Delta\tau^c_{\pi<c+a>}$)),
- two coefficients for the irradiation hardening and the strain softening of the basal CRSS (α_B the obstacle force and k_B the strain softening coefficient, the value $\rho_l(0) = N_0 d$ being fixed),
- two coefficients for the intra-granular kinematic hardening for the basal slip system (C_B and D_B),
- two tuning parameters, D and δ, for the empirical concentration rule that need to be fitted on the B–Z model whenever the intra-granular behavior is modified.

The other parameters fitted on the behavior of the non irradiated recrystallized zirconium alloys are not modified.

Two mechanical tests, performed at 350 °C, are used for the fitting: an internal pressure test ($\Sigma_{rr} \approx 0, \Sigma_{\theta\theta}, \Sigma_{zz} = \Sigma_{\theta\theta}/2$) performed on an irradiated cladding tube specimen made of M5® alloy and a transverse tensile test ($\Sigma_{\theta\theta}$) in the hoop direction performed on an irradiated cladding tube specimen made of recrystallized Zy-4. For the internal pressure test the hoop strain is accurately known during testing thanks to precise extensometers. The test is performed up to 0.8% total hoop strain at a strain rate of 3×10^{-4} s^{-1}. On the contrary, in the case of the transverse tensile test (in the hoop direction) which is performed by using a ring shaped specimen, only the displacement is recorded during testing. Moreover the specimen undergoes a slight bending at the beginning of the test. The test is performed at a strain rate of 1.6×10^{-4} s^{-1} at 350 °C until failure of the specimen. Irradiation and test conditions are given in Table 1.

As for the non irradiated material, the test is computed using the texture characteristic of recrystallized zirconium alloys cladding tubes (Fig. 1). Simultaneously, a transverse tensile test is computed, using the isotropic texture (Fig. 2(a)), in order to adjust both parameters D and δ on the local stress and strain obtained by the B–Z model.

In order to account for the reversal of the principal slip system shown by the TEM observations, the CRSS hierarchy is modified. The prism, the pyramidal <a> and the pyramidal <c + a> CRSS are more increased than the basal CRSS in order for the basal CRSS to be the lowest. As the plastic strain proceeds, the basal CRSS decreases from the initial basal CRSS of the irradiated material down to the basal CRSS of the unirradiated material due to loop clearing by moving dislocations.

5.3. Results of the refinement

The refined coefficients are given in Table 4. Firstly, it can be noticed on Fig. 5 that a good adjustment of the C–P model on the B–Z model is obtained ensuring that the C–P model is close to a self-consistent model both at the micro and macroscopic scale. It is also shown on Fig. 6 that the flow stress computed for the internal pressure test is slightly underestimated and the flow stress for the transverse tensile test is slightly over-estimated. The relative slip systems activities at 0.2% hoop plastic strain for the internal pressure test and the transverse tensile test are given in Table 5. It is shown that the basal slip is strongly activated for both internal pressure and transverse tensile tests (respectively 68% and 61%) in good agreement with the TEM observations. Nevertheless it can be noticed that the pyramidal <c + a> slip system is significantly activated (27%) for the internal pressure test in order to accommodate the high local stress in the "hard" grains. In addition, for the ring test, the pyramidal <a> slip system is also significantly

Table 4
Coefficients for the irradiated material obtained after the refinement.

Parameter	Value
Y^* (MPa)	80000
ν^*	0.4
n^*	10
K^* (MPa s$^{1/n}$)	5
τ^{c*}_P (MPa)	45
$\Delta\tau^c_P$ (MPa)	195
$\tau^{c*}_{\pi<a>}$ (MPa)	60
$\Delta\tau^c_{\pi<a>}$ (MPa)	180
$\tau^{c*}_{\pi<c+a>}$ (MPa)	140
$\Delta\tau^c_{\pi<c+a>}$	160
τ^{c0*}_B (MPa)	85
$\rho_b(0)^*$ (m^{-2})	5×10^{14}
α_B	0.5
k_B	40
C_B (MPa)	1×10^5
D_B	3000
D	280
δ	0.53

* Fixed coefficients.

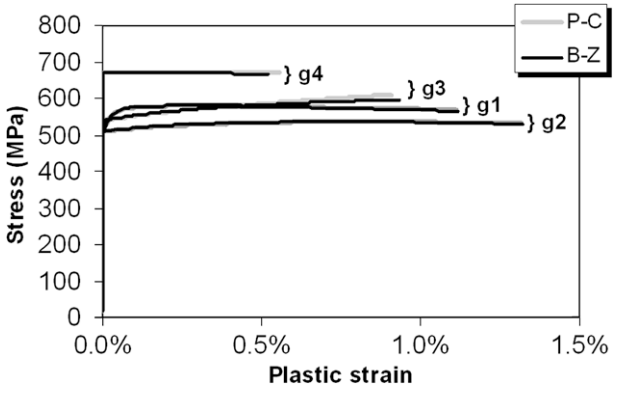

Fig. 5. Stress–plastic strain curves of four grains used for the adjustment of the C–P model on the self-consistent B–Z model. In gray lines is shown the B–Z model local response and in black lines the C–P model local response. The computed test is a transverse tensile test.

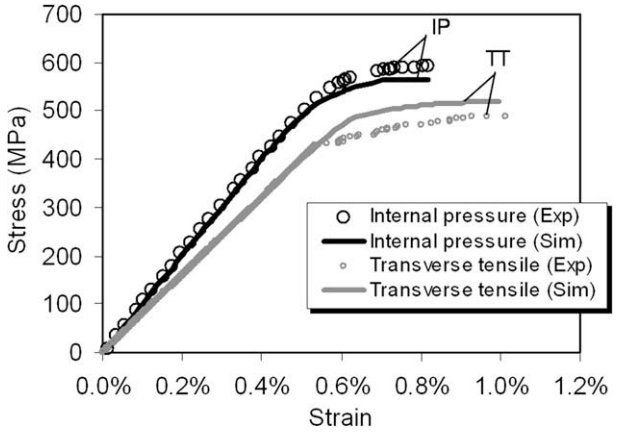

Fig. 6. Experimental (Exp) and Simulated (Sim) stress–strain curves of the Transverse Tensile test (TT) and the Internal Pressure test (IP) for the irradiated material.

Table 5
Slip system activities obtained at $E^p = 0.2\%$ for the irradiated material. In bold letters are indicated the principal slip systems.

Activity	Transverse tensile	Internal pressure
A_P	8%	1%
$A_{\pi<a>}$	31%	4%
A_B	**61%**	**68%**
$A_{\pi<c+a>}$	0%	27%

activated (31%). However, no pyramidal channel has been observed by TEM for transverse tensile tests and internal pressure tests. This could be explained, as pointed out previously, by the too "stiff" homogenization procedure. It is nevertheless possible that limited pyramidal slip occurs without significant clearing of loops.

The obstacle strength obtained for the basal slip system, $\alpha_B = 0.5$, is consistent with the literature data [70,8,71]. The increments in the CRSS obtained for the non basal slip systems also allow the estimation of the obstacle strength using Eq. (9) with $N = 5 \times 10^{22}\ m^{-3}$ and $d = 10$ nm. The obstacle strength for the prism slip, the pyramidal <a> slip and the pyramidal <c + a> slip are respectively 0.94, 0.87 and 0.78. These values seem to be overestimated according to the literature data.

The initial basal and prism CRSS ($\tau_B^c(0) = \tau_B^{c0} + \alpha_B \mu b \sqrt{\rho_i(0)} = 188$ MPa, $\tau_P^c = \tau_P^{c0} + \Delta\tau_P^c = 240$ MPa) obtained by fitting the polycrystalline model are higher than the CRSS estimated in [16] from the flow stress at 0.005% plastic strain. This is mainly due to the very low offset chosen in [16]. Nevertheless the differences between the basal and prismatic CRSS obtained in these two studies are similar.

5.4. Simulation of low cycle fatigue tests

In order to validate the approach, the polycrystalline model developed for irradiated recrystallized zirconium alloys is used to simulate low cycle fatigue tests that have not been used for the refinement. Low cycle fatigue tests in tension and compression along the transverse direction have been computed for both the unirradiated and the irradiated material, in agreement with the low cycle fatigue tests performed by Wisner et al. [39]. The first thirty and a quarter cycles are computed at a fixed total strain amplitude (where the term "amplitude" refers to half of the total peak-to-peak excursion according to [75], convention used in [39]) of $E = 1\%$ for the unirradiated material and $E = 0.9\%$ for the irradiated material. The stress–plastic strain curves are shown in Fig. 7 and compared to the experimental results obtained from the figures and the other experimental data given in [39]. The maximum tensile stress is recorded during the test and is reported in Fig. 8. The experimental data are also reported on Fig. 8 using both the figure and the number of cycles to failure given in [39]. It is shown on Fig. 7 that the model reproduces correctly the strong Bauschinger effect observed experimentally although it has only been adjusted on monotonic tests. It is also shown that the model reproduces the rapid cyclic softening observed experimentally for the irradiated material (Fig. 8), the softening rate being slightly higher in the modeling than in the experiment.

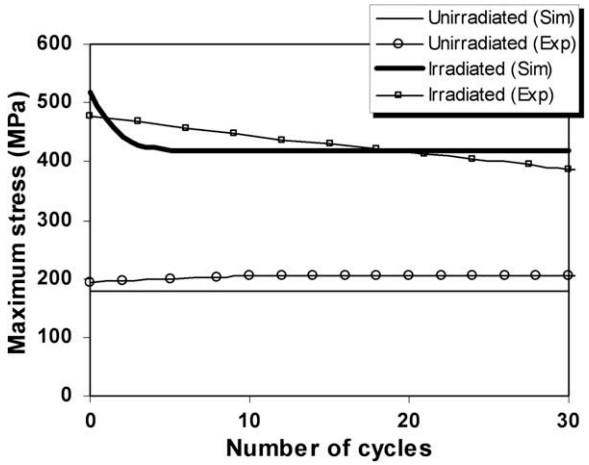

Fig. 8. Computed cyclic strain softening behavior of the irradiated recrystallized zirconium alloy in low cycle fatigue test with 0.9% total strain amplitude compared to the non irradiated material with 1% total strain amplitude. The computations (Sim) are compared to the experimental data (Exp) obtained from [39].

6. Discussion

Although the main objective of this work is to model the mechanical behavior of irradiated zirconium alloys, it is shown that the polycrystalline model proposed for the unirradiated recrystallized zirconium alloys gives satisfactory results. Indeed, it is seen that the macroscopic behavior computed by the model

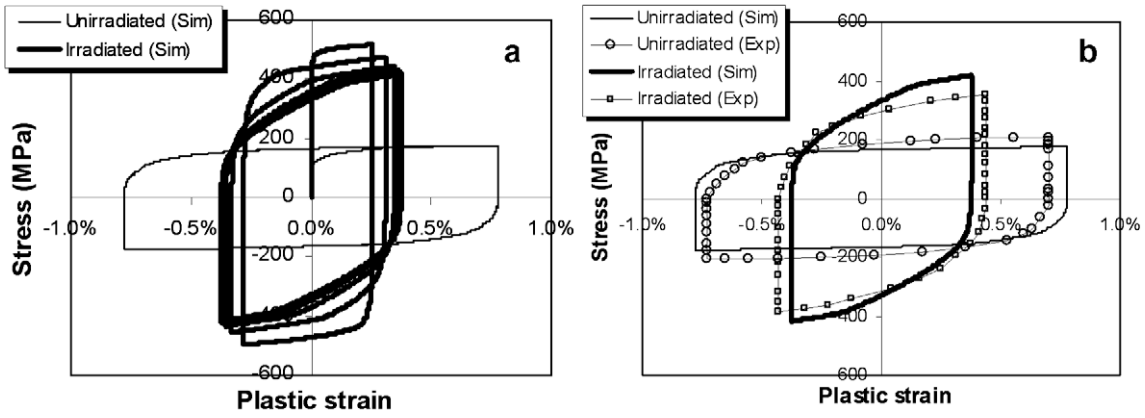

Fig. 7. (a) Simulated stress–plastic strain curves (Sim) for the non irradiated material and the irradiated material obtained during the computation of low cycle fatigue tests with respectively 1% and 0.9% total strain amplitude. (b) Stabilized hysteresis loops computed (Sim) after thirty and a quarter cycles for the unirradiated and the irradiated recrystallized material with respectively 1% and 0.9% total strain amplitude. The computation is compared to the experimental data (Exp) obtained from [39].

is in correct agreement with the experimental results obtained at 350°C despite the simple intra-granular behavior chosen (no intra-granular strain hardening). Only the flow stress computed for the axial tensile test is slightly underestimated. At the microscopic scale the relative slip system activities computed for the transverse tensile test and the axial tensile test are in agreement with the observed slip systems reported in the literature [14,27,26,58]. In the case of the internal pressure test the prism slip system activity is low and the basal slip activity is high which is in disagreement with the literature data. It has to be pointed out that the coefficients set obtained is not unique. Indeed, a better fit can be obtained for the macroscopic flow stress with different CRSS sets but in that case the relative slip system activities are in disagreement with the TEM observations. This disagreement is mainly due to the "secant" approximation used for the homogenization procedure. Better estimation of the slip system activities could probably be obtained by using an "affine" [47,68] or a "second order" [67] approximation. The low cycle fatigue test computed for the non irradiated material (Figs. 7 and 8) is in agreement with the results obtained by Wisner et al. [39] on RXA Zy-2 tested at 343 °C. Indeed, the Bauschinger effect is also reproduced as well as the nearly constant maximum stress measured during the low cycle fatigue test. The value of the flow stress is also in correct agreement with the experimental value.

The polycrystalline model adapted to the irradiated recrystallized zirconium alloys tested at 350 °C is also able to reproduce the macroscopic flow stress for the transverse tensile test and the internal pressure test. The flow stress is however slightly underestimated for the internal pressure test and slightly overestimated for the transverse tensile test. At the microscopic scale, the computed slip system activities show that the basal slip is mainly activated for transverse tensile test and internal pressure test, in good agreement with the TEM observations of basal channels for these two loading conditions. The modeling is thus able to reproduce, for the transverse tensile test, the change of principal slip system with neutron irradiation. However, the important activation of other slip systems, such as the pyramidal <*a*> glide for transverse tensile test and the pyramidal <*c* + *a*> glide for internal pressure test, indicates that the polycrystalline model tends to overestimate the activities of the secondary slip systems. The low cycle fatigue test computed for the irradiated material is also in good agreement with the results obtained by Wisner et al. [39] on Zy-2 tested at 343 °C. Indeed, a strong Bauschinger effect is also reproduced as well as the important cyclic strain softening observed. The computed values of the flow stress are in good agreement with the experimental results. The magnitude of the strain softening seems however to be slightly underestimated and the strain softening rate is slightly overestimated by the model compared to the experimental results.

The good agreement obtained between the computation of the low cycle fatigue tests and the experimental results suggests that the main features of the mechanical behavior of the irradiated material have been captured by the polycrystalline model. Indeed, by attributing all the intra-granular strain hardening to the intra-granular kinematic strain hardening (on the basal slip system), and adjusting the kinematic strain hardening behavior only on monotonic loading, the model gives a satisfactory cyclic response. This confirms that the observed strain hardening is mainly due to the kinematic strain hardening in irradiated zirconium alloys in good agreement with the experimental analysis described in the first part of the paper. The introduction of the intra-granular strain softening is also able to reproduce the cyclic softening observed although during monotonic loading the strain softening is not observed at the macroscopic scale, in agreement with the experimental results.

Improvement of the modeling can probably be achieved by using more accurate self-consistent models ("affine" or "second order" estimates) [47,67], leading to a lower activation of the secondary slip systems. In addition, models that are not restricted to elasto-plastic behavior could be used to compute the strain rate sensitivity as well as stress relaxation tests [43]. The model proposed here is also restricted to transverse tensile tests and internal pressure tests since only the basal channeling is taken into account. In order to compute axial tensile tests prism and pyramidal channeling must also be taken into account in the modeling.

Compared to macroscopic models [43,36,76,77], this polycrystalline model has the great advantage to compute explicitly the kinematic strain hardening as a consequence of the interaction between the grains instead of a full empirical kinematic strain hardening. The isotropic strain hardening, consequence of the evolution of the various CRSS, is also modeled more physically by taking into account the activation of the different slip systems, such as the main activation of the basal slip in the case of the irradiated material.

7. Conclusions

The objective of this work was to propose the first polycrystalline modeling for neutron irradiated zirconium alloys based on the microscopic deformation mechanisms.

Firstly, an analysis based on various experimental data has been performed, both at the microscopic and at the macroscopic scale. It has been discussed that the kinematic strain hardening is significantly increased due to the plastic strain localization inside the dislocation channels as well as the only basal slip activation observed for internal pressure tests and transverse tensile tests. This explains that macroscopic strain hardening is observed although inside the channels strain softening occurs. This also accounts for the presence of the channels before the yield drop observed for the transverse tensile test.

Then, the first polycrystalline model adapted to irradiated zirconium alloys, that takes into account the change in the deformation mechanisms due to irradiation, has been developed. The irradiation induced hardening has been taken into account by increasing the critical resolved shear stresses of all slip systems. In order to take into account the reversal of the principal slip system, the non basal CRSS have been more increased than the basal CRSS. In addition, the dislocation channeling mechanism has been modeled by taking into account the strain softening of the basal CRSS occurring inside basal channels. A non linear kinematic strain hardening term, which increases with basal slip, has also been introduced at the grain scale. The model reproduces the mechanical behavior for internal pressure tests and transverse tensile tests, in agreement with the slip system activities observed by TEM. Low cycle fatigue tests in the transverse direction have been simulated and compared to the experimental results obtained by Wisner et al. [39]. The simulated tests are in good agreement with the experimental results. The strong Bauschinger effect observed after irradiation is reproduced as well as the significant cyclic strain softening. The fact that this novel physically based model is able to reproduce this variety of testing conditions shows that this model captures the main features of the mechanical behavior of the irradiated material. This original polycrystalline model, the first proposed for neutron irradiated metals, constitutes a step toward a fully predictive modeling of the behavior of irradiated zirconium alloys.

Acknowledgements

Acknowledgements are given to P. Pilvin for discussions concerning the polycrystalline modeling. The authors also want to thank AREVA-NP and EDF for supporting this study.

Appendix: Notations, equations of the polycrystalline model and symbols

Notations

The scalar quantity $\|\underline{x}\|$, where $\underline{x}$ is a second rank tensor, is defined as $\|\underline{x}\| = \sqrt{\frac{2}{3}\underline{x} : \underline{x}}$. The constricted product $\underline{x} : \underline{y}$ is defined by $\underline{x} : \underline{y} = \sum_i \sum_j x_{ij} y_{ij}$.

The scalar quantity $J_2(\underline{x})$ is given by $J_2(\underline{x}) = \sqrt{\frac{3}{2} dev(\underline{x}) : dev(\underline{x})}$, where dev($\underline{x}$) is the deviator of a second rank tensor which is defined as $dev(\underline{x}) = \underline{x} - \frac{1}{3} tr(\underline{x}) \underline{I}$. The tensor $\underline{I}$ is the identity second rank tensor. Its components are equal to δ_{ij}, where δ_{ij} is the Kronecker's symbol. The scalar quantity tr($\underline{x}$) is the trace of the second rank tensor $\underline{x}$ and is equal to $tr(\underline{x}) = \sum_i x_{ii}$. The fourth rank tensor I which appears in the Hooke's law corresponds to the symmetrical identity fourth rank tensor with components $(\delta_{ik}\delta_{jl} + \delta_{il}\delta_{jk})/2$. The components of the fourth rank tensor $\underline{I} \otimes \underline{I}$ can be expressed as $\delta_{ij}\delta_{kl}$. The components of the second rank tensor $n_s \otimes m_s + m_s \otimes n_s$ are $n_i m_j + n_j m_i$. The notation appearing into the flow law $\langle x \rangle$ is defined as $\langle x \rangle = 0$ if $x < 0$ and $\langle x \rangle = x$ when $x \geqslant 0$. The notation sign(x) correspond to the sign of the scalar quantity x and can be expressed as sign(x) = $x/|x|$.

Equations of the polycrystalline model adapted to the irradiated material

Averaging relationships and Hooke's law

$$\underline{\underline{E}}^p = \sum_{g \in G} f_g \underline{\underline{\varepsilon}}^p_g; \quad \underline{\underline{\Sigma}} = \sum_{g \in G} f_g \underline{\underline{\sigma}}_g = 2\mu \left\{ \mathbf{I} + \frac{\nu}{1-2\nu} \underline{\underline{I}} \otimes \underline{\underline{I}} \right\} (\underline{\underline{E}} - \underline{\underline{E}}^p)$$

Concentration rule:

$$\underline{\underline{\sigma}}_g = \underline{\underline{\Sigma}} + 2\mu(1-\beta)(\underline{\underline{B}} - \underline{\underline{\beta}}_g) \text{ with } \underline{\underline{B}} = \sum_{g \in G} f_g \underline{\underline{\beta}}_g \text{ and } \beta = \frac{2(4-5\nu)}{15(1-\nu)}$$

$$\dot{\underline{\underline{\beta}}}_g = \dot{\underline{\underline{\varepsilon}}}^p_g - D(\underline{\underline{\beta}}_g - \delta \underline{\underline{\varepsilon}}^p_g) \|\dot{\underline{\underline{\varepsilon}}}^p_g\|$$

Intra-granular constitutive behavior:
Resolved shear stress:

$$\tau_s = \frac{1}{2} \underline{\underline{\sigma}}_g : (\underline{n}_s \otimes \underline{m}_s + \underline{m}_s \otimes \underline{n}_s)$$

Plastic strain rate of the grain:

$$\dot{\underline{\underline{\varepsilon}}}^p_g = \frac{1}{2} \sum_{s \in S} \dot{\gamma}_s (\underline{n}_s \otimes \underline{m}_s + \underline{m}_s \otimes \underline{n}_s)$$

Flow law:

$$\dot{\gamma}_s = \left\langle \frac{|\tau_s - x_s| - \tau^c_s}{K} \right\rangle^n \text{sign}(\tau_s - x_s)$$

Evolution of the CRSS: irradiation induced hardening and strain softening for the basal slip

$$\tau^c_s = \tau^{c0}_s + \Delta\tau^c_s \quad \text{with} \quad \Delta\tau^c_s \quad \text{being constant for } s \neq B$$
$$\tau^c_B = \tau^{c0}_B + \alpha_B \mu b \sqrt{\rho_l} \quad \text{with} \quad \rho_l = Nd \quad \text{for the basal slip}$$
$$\frac{d\rho_l}{dt} = -k_B \rho_l \left[\sum_{s \in B} |\dot{\gamma}_s| \right] \quad \text{with} \quad \rho_l(0) = N_0 d$$

Intra-granular kinematic strain hardening for the basal slip:
$\dot{x}_s = C_B \dot{\gamma}_s - D_B x_s |\dot{\gamma}_s|$ for the basal slip systems ($s \in B$), with $x_s(t = 0) = 0$ and $x_s = 0$ for non basal slip systems ($s \neq B$).

Table of symbols used in the polycrystalline model

Symbol	Units	Variables and coefficients
$\underline{\underline{\Sigma}}$	MPa	Macroscopic stress
$\underline{\underline{E}}, \underline{\underline{E}}^p$	–	Macroscopic strain and macroscopic plastic strain
$\underline{\underline{\sigma}}_g$	MPa	Local stress
$\underline{\underline{\varepsilon}}^p_g, \underline{\underline{\varepsilon}}^p_g$	–	Local plastic strain and local plastic strain rate
β_g, $\underline{\underline{\beta}}_g$	–	Internal variable for the concentration rule and its time derivative
f_g	–	Volume fraction of the crystallographic phase
τ_s	MPa	Resolved shear stress on the s slip system
x_s	MPa	Intra-granular kinematic stress on the s slip system
$\dot{\gamma}_s$	s^{-1}	Shear strain rate on the s slip system
$\underline{m}_s$	–	Glide direction
$\underline{n}_s$	–	Normal direction of the slip plane
Y	MPa	Elasticity coefficients (Young's modulus,
ν	–	Poisson's ratio)
n^*	–	Coefficients of the flow law
K^*	MPa $s^{1/n}$	
τ^c_s	MPa	Critical resolved shear stress (CRSS)
$\Delta\tau^c_s$(*for* $s \neq B$)	MPa	Increment in the CRSS for non basal slip systems
$\rho_l(0) = N_0 d^*$	m^{-2}	Irradiation defects density
α_B	–	Obstacle force for the basal slip
k_B	–	Strain softening coefficient for the basal slip
C_B	MPa	Coefficients of the intra-granular
D_B	–	kinematic strain hardening for the basal slip
D	–	Tuning coefficients for the empirical
δ	–	concentration rule

*Fixed coefficients.

References

[1] D.O. Northwood, R.W. Gilbert, L.E. Bahen, P.M. Kelly, R.G. Blake, A. Jostsons, P.K. Madden, D. Faulkner, W. Bell, R.B. Adamson, J. Nucl. Mater. 79 (1979) 379.
[2] M. Griffiths, J. Nucl. Mater. 159 (1988) 190.
[3] H.R. Higgy, F.H. Hammad, J. Nucl. Mater. 44 (1972) 215.
[4] C.J. Baroch, in: Properties of Reactor Structural Alloys after Neutron or Particle Irradiation, ASTM STP 570, 1975, p. 129.
[5] T. Yasuda, M. Nakatsuka, K. Yamashita, in: Zirconium in the Nuclear Industry: 7th International Symposium, ASTM STP 939, 1987, p. 734.
[6] G. Saada, J. Washburn, Symp. J. Phys. Soc. Jpn. 18 (Suppl. 1) (1963) 43.
[7] A.J.E. Foreman, J.V. Sharp, Philos. Mag. 19 (1969) 931.
[8] P.B. Hirsch, in: Proceedings of a Conference on Point Defect Behavior and Diffusional Processes, University of Bristol, 13–16 September 1976.
[9] C.E. Coleman, D. Mills, J. van der Kuur, Canad. Metall. Quart. 11 (1972) 91.
[10] C.D. Williams, R.B. Adamson, K.D. Olhausen, in: European Conference on Irradiation Behavior of Fuel Cladding and Core Component Materials, Karlsruhe, 1974, p. 189.
[11] T. Onchi, H. Kayano, Y. Higashiguchi, J. Nucl. Mater. 88 (1980) 226.
[12] K. Pettersson, J. Nucl. Mater. 105 (1982) 341.
[13] R.B. Adamson, W.L. Bell, in: Microstructure and Mechanical Behavior of Materials, International Symposiums, vol. 1, Xian, China, 1985, p. 237.
[14] M. Fregonese, C. Régnard, L. Rouillon, T. Magnin, F. Lefebvre, C. Lemaignan, in: Zirconium in Nuclear Industry: 12th International Symposium, ASTM STP 1354, 2000, p. 377.
[15] C. Régnard, B. Verhaeghe, F. Lefebvre-Joud, C. Lemaignan, in: Zirconium in the Nuclear Industry: 13th International Symposium, ASTM STP 1423, 2002, p. 384.
[16] F. Onimus, I. Monnet, J.L. Béchade, C. Prioul, P. Pilvin, J. Nucl. Mater. 328 (2004) 165.
[17] M.S. Wechsler, Dislocation Channeling in Irradiated and Quenched Metals. The Inhomogeneity of Plastic Deformation, ASM, Metals Park, Ohio, 1973. p. 19.
[18] D. Rodney, G. Martin, Y. Bréchet, Mater. Sci. Eng. A 309–310 (2001) 198.
[19] G.R. Odette, M.Y. He, E.G. Donahue, P. Spätig, T. Yamamoto, J. Nucl. Mater. 307–311 (2002) 171.
[20] T.S. Byun, N. Hashimoto, J. Nucl. Mater. 354 (2006) 123.

[21] A. Luft, Microstructural processes of plastic instabilities in strengthened metals, Prog. Mater. Sci. 35 (1991) 97.
[22] D.J. Edwards, B.N. Singh, J.B. Bilde-Sørensen, J. Nucl. Mater. 342 (2005) 164.
[23] F. Onimus, J.L. Béchade, C. Prioul, P. Pilvin, I. Monnet, S. Doriot, B. Verhaeghe, D. Gilbon, L. Robert, L. Legras, J.P. Mardon, J. ASTM Int. (JAI) 2 (8) (2005) 24.
[24] D.L. Douglass, The Metallurgy of Zirconium. Atomic Energy Review Supplement, International Atomic Energy Agency, Vienna, 1971, p. 41.
[25] E. Tenckhoff, Deformation mechanisms, texture, and anisotropy in zirconium and Zircaloy, ASTM STP 966, 1988.
[26] F. Ferrer, A. Barbu, T. Bretheau, J. Crépin, F. Willaime, D. Charquet, in: Zirconium in Nuclear Industry, 13th International Symposium, ASTM STP 1423, 2002, p. 863.
[27] R. Brenner, J.L. Béchade, O. Castelnau, B. Bacroix, J. Nucl. Mater. 305 (2002) 175.
[28] J.V. Sharp, Radiat. Effects Defects Solids 14 (1972) 71.
[29] R.E. Voskoboynikov, Y.N. Osetsky, D.J. Bacon, Mater. Sci. Eng. A 400–401 (2005) 49.
[30] R.E. Voskoboynikov, Y.N. Osetsky, D.J. Bacon, Mater. Sci. Eng. A 400–401 (2005) 54.
[31] T. Nogaret, C. Robertson, D. Rodney, Philos. Mag. 87 (6) (2007) 945.
[32] T. Nogaret, D. Rodney, M. Fivel, C. Robertson, J. Nucl. Mater. 380 (2008) 22.
[33] S.R. MacEwen, C.E. Ells, O.T. Woo, J. Nucl. Mater. 101 (1981) 336.
[34] N. Christodoulou, Acta Metall. 37 (2) (1989) 529.
[35] Z.H.A. Kassam, Z. Wang, Mater. Sci. Eng. A 171 (1993) 55.
[36] P. Delobelle, P. Robinet, P. Geyer, P. Bouffioux, J. Nucl. Mater. 238 (1996) 135.
[37] J. Crépin, T. Bretheau, D. Caldemaison, F. Ferrer, Acta Mater. 48 (2000) 505.
[38] C. Li, S. Ying, B. Shen, S. Qui, X. Ling, Y. Wang, Q. Peng, J. Nucl. Mater. 321 (2003) 60.
[39] S.B. Wisner, M.B. Reynolds, R.B. Adamson, in: Zirconium in the Nuclear Industry: 10th International Symposium, ASTM STP 1245, 1994, p. 499.
[40] R.B. Adamson, Philos. Mag. 17 (1968) 681.
[41] H.S. Rosenbaum, G.F. Rieger, D. Lee, Metall. Trans. 5 (1974) 1867.
[42] D. Lee, R.B. Adamson, in: Zirconium in the Nuclear Industry, ASTM STP 633, 1977, p. 385.
[43] F. Onimus, J.L. Béchade, C. Duguay, D. Gilbon, P. Pilvin, J. Nucl. Mater. 358 (2006) 176.
[44] M. Berveiller, A. Zaoui, J. Mech. Phys. Solids 26 (1979) 325.
[45] U.F. Kocks, C.N. Tomé, H.-R. Wenk, Texture and Anisotropy, first Ed., Preferred Orientations in Polycrystals and their Effect on Materials Properties, Cambridge University, 1998.
[46] F. Barbe, L. Decker, D. Jeulin, G. Cailletaud, Int. J. Plast. 17 (4) (2001) 513.
[47] R. Brenner, R. Masson, O. Castelnau, A. Zaoui, Eur. J. Mech. A/Solids 21 (2002) 943.
[48] T. Hoc, S. Forest, Int. J. Plast. 17 (2001) 65.
[49] G. Cailletaud, Int. J. Plast. 8 (1992) 55.
[50] P. Pilvin, in: Proceedings of the International Conference on Biaxial/Multiaxial Fatigue ESIS/SF2M, 1994, p. 31.
[51] J. Lemaitre, J.L. Chaboche, Mechanics of Solid Materials, Cambridge University, 1990.
[52] J.W. Hutchinson, Metall. Trans. A 8 (1977) 1465.
[53] R.A. Lebensohn, C.N. Tomé, Acta Metal Mater. 41 (9) (1993) 2611.
[54] P.A. Turner, C.N. Tomé, C.H. Woo, Philos. Mag. A 70 (4) (1994) 689.
[55] P.A. Turner, N. Christodoulou, C.N. Tomé, Int. J. Plast. 11 (3) (1995) 251.
[56] N. Letouzé, R. Brenner, O. Castelnau, J.L. Béchade, M.H. Mathon, Scripta Mater. 47 (2002) 595.
[57] P. Geyer, Ph.D. Thesis, Ecole des Mines de Paris, 1999.
[58] P. Geyer, X. Feaugas, P. Pilvin, in: Proceedings of Plasticity'99, Cancun, 1999.
[59] O. Fandeur, P. Pilvin, C. Prioul, J. Phys. IV France 11 (2001) 109.
[60] A. Akhtar, J. Nucl. Mater. 47 (1973) 79.
[61] P. Merle, J. Nucl. Mater. 144 (1987) 275.
[62] H. Numakura, Y. Minonishi, M. Koiwa, Philos. Mag. A 63 (5) (1991) 1077.
[63] G. Monnet, B. Devincre, L.P. Kubin, Acta Mater. 52 (2004) 4317.
[64] A. Andrade-Campos, S. Thuillier, P. Pilvin, F. Teixeira-Dias, Int. J. Plast. 23 (2007) 1349.
[65] A. Molinari, S. Ahzi, R. Kouddane, Mech. Mater. 26 (1997) 43.
[66] O. Castelnau, H. Francillette, B. Bacroix, R.A. Lebensohn, J. Nucl. Mater. 297 (2001) 14.
[67] P. Ponte Castaneda, J. Mech. Phys. Solids 44 (6) (1996) 827.
[68] A. Zaoui, R. Masson, Mater. Sci. Eng. A 285 (2000) 418.
[69] R.A. Lebensohn, Y. Liu, P. Ponte Castaneda, Acta Mater. 52 (2004) 5347.
[70] L.M. Brown, R.K. Ham, in: A. Kelly, R.B. Nicholson (Eds.), Strengthening Methods in Crystals, Applied Science Publishers Ltd., 1971, p. 9.
[71] G.S. Was, in: Fundamentals of Radiation Materials Science, Springer Verlag, 2007, p. 594.
[72] C. Pokor, X. Averty, Y. Bréchet, P. Dubuisson, J.P. Massoud, Scripta Mater. 50 (5) (2004) 597.
[73] L. Meric, P. Poubanne, G. Cailletaud, J. Eng. Mater. Technol. (Trans. ASME) 113 (1) (1991) 162.
[74] Y. Jiang, P. Kurath, Int. J. Plast. 12 (3) (1996) 387.
[75] W.J. O'Donnell, B.F. Langer, Nucl. Sci. Eng. 20 (1964) 1.
[76] I. Schäffler, P. Geyer, P. Bouffioux, P. Delobelle, J. Eng. Mater. Technol. 122 (2000) 168.
[77] J.W. Dunlop, Y.J.M. Bréchet, L. Legras, Y. Estrin, Mater. Sci. Eng. A (2007) 77.